

Quantum Chemical and Statistical Rate Investigation of the $\text{CF}_2(\text{a}^3\text{B}_1) + \text{NO}(\text{X}^2\Pi)$ Reaction: A Fast Chemical Quenching Process[†]

Thanh Lam Nguyen, Shaun A. Carl, Minh Tho Nguyen,* and Jozef Peeters

Department of Chemistry, University of Leuven, Celestijnenlaan 200 F, B-3001-Leuven, Belgium

Received: December 2, 2006; In Final Form: January 25, 2007

The reaction of $\text{CF}_2(\text{a}^3\text{B}_1)$ with $\text{NO}(\text{X}^2\Pi)$ was theoretically investigated using the B3LYP, MP2, CCSD(T), G2M, CASSCF, and CASPT2 quantum chemical methods with various basis sets including 6-31G(d), 6-311G(d), 6-311+G(3df), cc-pVDZ, and cc-pVTZ. In agreement with the experimental kinetic data, the $\text{CF}_2(\text{a}^3\text{B}_1) + \text{NO}(\text{X}^2\Pi)$ reaction is found to proceed via a fast, barrier-free combination. This process, occurring on the doublet potential energy surface, leads to the electronically excited adduct $\text{F}_2\text{C}-\text{NO}(\text{2}^2\text{A}'')$, which readily undergoes a surface hopping to the $1^2\text{A}'$ electronic surface, with a Landau–Zener transition probability estimated to be close to 90% per C–N vibration. The metastable adduct $\text{F}_2\text{C}-\text{NO}(\text{1}^2\text{A}')$ can then either spontaneously decompose into $\text{CF}_2(\text{X}^1\text{A}_1) + \text{NO}(\text{X}^2\Pi)$ in a direct chemical quenching mechanism or relax to its ground-state equilibrium structure $\text{F}_2\text{CNO}(\text{X}^2\text{A}')$. The product distribution resulting from the latter, chemically activated intermediate was evaluated by solution of the master equation (ME), under different reaction conditions, using the exact stochastic simulation method; microcanonical rate constants were computed using Rice–Ramsperger–Kassel–Marcus (RRKM) theory, based on the potential energy surfaces (PESs) constructed using both G2M and CASPT2 methods. The RRKM/ME analysis reveals that the hot $\text{F}_2\text{CNO}(\text{X}^2\text{A}')$ rapidly fragments almost exclusively to the same products as above, $\text{CF}_2(\text{X}^1\text{A}_1) + \text{NO}(\text{X}^2\Pi)$, which amounts to an indirect chemical quenching mechanism. The reaction on the quartet PES is unlikely to be significant except at very high temperatures. The high crossing probability (up to 90%) between the two “avoided” doublet PESs points out the inherent difficulty in treating chemically activated reactions with fast-moving nuclei within the Born–Oppenheimer approximation.

I. Introduction

Whereas methylene (CH_2), the simplest carbene, has a triplet electronic ground state with a singlet–triplet energy gap of 9 kcal mol⁻¹,¹ difluoromethylene (CF_2) has a closed-shell singlet electronic ground state $^1\text{A}_1$ that^{2,3} lies 56.6 kcal mol⁻¹ lower in energy than the triplet excited state $^3\text{B}_1$. This is due to the strong stabilization of the fluorocarbene through $p\pi$ back-donation, rendering the singlet state almost unreactive.⁴ The triplet state, however, is not only much more reactive, but with a radiative lifetime of about 1 s,^{5,6} it is expected to play a significant role in the chemistry of fluorocarbon etching plasmas, used in the production of integrated circuits. Recent calculations by Tennyson et al.⁷ on the $e + \text{CF}_2$ collision revealed rather large cross sections of up to 1×10^{-20} m² at 6 eV, indicating that considerable concentrations of $\text{CF}_2(\text{a}^3\text{B}_1)$ could be built up in a fluorocarbon plasma. In this context, a detailed understanding of the gas-phase reaction mechanisms and kinetics of the metastable species $\text{CF}_2(\text{a}^3\text{B}_1)$ is required to further optimize the etching process.

In our previous experiments,⁸ $\text{CF}_2(\text{a}^3\text{B}_1)$ radicals were generated by pulsed laser photolysis of $\text{C}_2\text{F}_4(\text{X}^1\text{A}_g)$ at 193 nm. The overall thermal rate constants of the $\text{CF}_2(\text{a}^3\text{B}_1)$ reactions with NO and H_2 were measured over the 287–600 K temperature range. The measured rate coefficient of $(9.7 \pm 2.5) \times 10^{-12} \exp[+(545 \pm 80) \text{ K}/T]$ cm³ s⁻¹ for the $\text{CF}_2(\text{a}^3\text{B}_1) + \text{NO}$ reaction⁸ shows the reaction to be very fast and to have a marked negative temperature dependence, indicating that the initial

reaction step is a barrierless addition process. For the reaction of $\text{CF}_2(\text{a}^3\text{B}_1) + \text{H}_2$,⁸ only an upper limit rate constant of $k \leq 3 \times 10^{-14}$ cm³ s⁻¹ could be established,^{8a} and this was demonstrated to result mainly from a hydrogen abstraction of H_2 by triplet CF_2 giving $\text{CF}_2\text{H} + \text{H}$.^{8b} Although overall thermal rate coefficients could be measured with good accuracy and the absolute values and temperature dependence provided some indication of the reaction mechanisms involved,^{8a} experimental evaluation of the product distribution is a far more difficult task. In such a case, quantum chemical (QC) calculations, in combination with the Rice–Ramsperger–Kassel–Marcus (RRKM) rate theory, are most helpful tools to unravel the underlying reaction processes and to obtain quantitative information on the product distribution.

In this work, the $\text{CF}_2(\text{a}^3\text{B}_1) + \text{NO}$ reaction, which has not yet been studied theoretically as far as we are aware, was investigated in depth. Note that the analogous $\text{CH}_2(\text{X}^3\text{B}_1) + \text{NO}$ reaction, which plays an important role in the NO_x reburning processes for the reduction of NO emissions in hydrocarbon combustion, has been theoretically and experimentally studied in detail.^{9–11}

II. Theoretical Methods

II.1. Quantum Chemical Calculations. Local minima and transition structures (TSs) on the potential energy surfaces (PESs) were initially optimized using density functional theory with the hybrid B3LYP functional¹² in conjunction with the 6-31G(d) basis set (here, only the five “pure-d” basis functions were used). The unrestricted formalism (UHF, UB3LYP) was

[†] Part of the special issue “M. C. Lin Festschrift”.

* Corresponding author. E-mail: minh.nguyen@chem.kuleuven.be.

TABLE 1: Calculated Total and Zero-Point Energies (hartree) and Relative Energy (kcal mol⁻¹) Using the B3LYP/6-311+G(3df) and G2M Levels of Theory

species	total energy			relative energy		
	B3LYP ^a	G2M	ZPE ^b	B3LYP ^a	G2M	exp ^c
CF ₂ (a ³ B ₁) + NO(X ² Π)	-367.64672	-367.02731	0.01134	0.0	0.0	0.0
CF ₂ (X ¹ A ₁) + NO(X ² Π)	-367.73046	-367.11712	0.01151	-52.4	-56.4	-54 ± 2.9 ^e -56.6 ^g -67 ± 2.9
N(⁴ S) + F ₂ CO(X ¹ A ₁)	-367.73876	-367.13223	0.01414	-56.0	-65.8	
N(² D) + F ₂ CO(X ¹ A ₁)	-367.63832	-367.03246	0.01414	7.0	-3.2	
F(² P) + FCON(¹ A')	-367.51218		0.01054	83.9		
F(² P) + FCON(³ A'')	-367.55657		0.01033	55.9		
F(² P) + FCNO(¹ A')	-367.63165		0.01347	10.8		
F(² P) + c-FCNO(¹ A')	-367.64596		0.01325	1.7		
F(² P) + FNCO(¹ A')	-367.67773	-367.05369	0.01344	-18.2	-16.6	
F ₂ N(² B ₁) + CO(X ¹ Σ _g)	-367.72459	-367.10729	0.01109	-49.0	-50.2	-49.8 ± 1.5
FN(X ³ Σ _g) + FCO(X ² A')	-367.68051	-367.05726	0.01097	-21.4	-18.8	
O(³ P) + F ₂ CN(X ² B ₂)	-367.65345	-367.03450	0.01313	-3.1	-4.5	
Iso1: F ₂ CNO(⁴ A)	-367.70790	-367.07533	0.01603	-35.5	-30.1	
Iso2: F ₂ CON(⁴ A)	-367.69136	-367.06583	0.01522	-25.6	-24.2	
Iso3a: F ₂ CNO(X ² A')	-367.78036	-367.14786	0.01733	-80.2	-75.6	
Iso3b: F ₂ CNO(² A'')	-367.76820	-367.13760	0.01750	-72.4	-69.2	
Iso4: c-F ₂ CNO(X ² A'')	-367.77383	-367.15466	0.01728	-76.1	-79.9	
Iso5: O=C(F)NF(X ² A'')	-367.78070	-367.15436	0.01678	-80.7	-79.7	
Iso6: F ₂ NCO(² A)	-367.68867	-367.06263	0.01475	-24.2	-22.2	
Iso7a: F ₂ CON(² A)	-367.70034		0.01526	-31.2	-31.5 ^f	
Iso7b: F ₂ CON(² A'')	-367.66758	-367.03756	0.01558	-10.5	-6.4	
TS1 (⁴ A'')					1.3 ^d	
TS2 (⁴ A)	-367.64157	-367.01119	0.01229	3.8	10.1	
TS3 (⁴ A'')	-367.65097	-367.01708	0.01344	-1.4	6.4	
TS4 (⁴ A'')	-367.66377	-367.03728	0.01291	-9.7	-6.3	
TS5 (² A)	-367.72971	-367.10721	0.01284	-51.2	-50.1	
TS6 (² A)	-367.72986	-367.10480	0.01579	-49.4	-48.6	
TS7 (² A)	-367.68787		0.01446	-23.9	-24.2 ^f	
TS8 (² A)	-367.68077	-367.04572	0.01407	-19.7	-11.6	
TS9 (² A)	-367.68735		0.01328	-24.3	-24.2 ^f	
TS10 (² A)	-367.68744	-367.06411	0.01317	-24.4	-23.1	

^a At the B3LYP/6-311+G(3df) level of theory. ^b Calculated at the B3LYP/6-31G(d_{5a}) level of theory and unscaled. ^c <http://srdata.nist.gov/cccbdb/>. ^d Based on the MP2/6-311+G(d)-optimized geometry. ^e Platz et al.⁴⁴ ^f Relative energy as compared to Iso3a F₂CNO(X²A'). ^g Koda² and Mckellar et al.³

used for open-shell species. Analytical harmonic vibration frequencies were then computed at this level to verify the character of the stationary points located (one imaginary frequency for a TS and all real frequencies for a minimum). Zero-point energies (ZPEs), scaled¹³ by a factor of 0.9806, were used to correct the relative energies. Geometries of the relevant stationary points were re-optimized using the same B3LYP method but with the larger 6-311+G(3df) basis set. Where necessary, vibrational analysis and intrinsic reaction coordinate (IRC) calculations were undertaken at the latter level to establish the correct connections between the reaction intermediates. To obtain more accurate relative energies, the coupled-cluster theory CCSD(T) method,¹⁴ in combination with the 6-311G(d) basis set, was also used to compute single-point electronic energies based on the B3LYP/6-311+G(3df)-optimized geometries. Direct CCSD(T)/6-311+G(3df) calculations for the systems under consideration could not be carried out because of the limits of our computational resources. Therefore, approximate CCSD(T)/6-311+G(3df) energies were evaluated using an additivity scheme based on the MP2 energies.¹⁵ In this additivity approximation, known as the G2M method,¹⁶ the total energy of a molecular system is computed as follows

$$E(\text{G2M}) = E[\text{CCSD(T)/6-311G(d)//B3LYP}_L] + \{E[\text{MP2/6-311+G(3df)//B3LYP}_L] - E[\text{MP2/6-311G(d)//B3LYP}_L]\} + 0.9806 \times \text{ZPE}[\text{B3LYP/6-31G(d)}]$$

where B3LYP_L stands here for the geometries at the B3LYP/6-311+G(3df) level. It was shown¹⁶ that the G2M relative

energies approach those derived from full CCSD(T)/6-311+G(3df) computations and can reproduce several molecular properties such as heats of formation, ionization energies, electron affinities, and reaction enthalpies within a chemical accuracy of 2 kcal mol⁻¹ for a large series of small molecules.¹⁷ The relative energies obtained at the G2M and B3LYP levels are comparable (see Table 1). However, where experimental data are available, the G2M values are found to be in closer agreement with experiment.

Some stationary points in this reaction system have wavefunctions strongly perturbed by spin-contamination effects in the unrestricted UHF formalism and/or have T1 diagnostic values much larger than 0.02 in the CCSD calculations, which is the recommended safe limit.¹⁸ The wavefunctions of these structures are likely to exhibit a multireference character or near-degeneracy. In this case, the multireference CASSCF method, in combination with the correlation-consistent cc-pVDZ basis set, was used to re-optimize geometries, and analytical Hessian calculations were also performed. Active spaces for the [CF₂-NO] system were chosen as 11 electrons distributed in 11 active orbitals, denoted as CASSCF(11,11). The active electrons chosen for the [CF₂NO] system include two σ(C-F), two σ(C-N), two σ(N-O), two lone pairs of O, two lone pairs of N, and one unpaired electron at C. These active spaces appear to be efficient and flexible enough to describe the different isomerization or dissociation processes involved. The most important configuration coefficients in the wavefunction for a considered species in the CASSCF(11,11) calculations are given in the Supporting Information. It should be noted here that, for

the stationary points for which the HF wavefunction is dominated by a single configuration, the CCSD(T) energies are the preferred choice over the CASPT2 calculations. To include dynamic correlations, the CASPT2/cc-pVTZ method¹⁹ with the same active spaces was employed to compute energies based on the CASSCF(11,11) reference wavefunctions.

To investigate the entrance channel of addition of CF₂(a³B₁) onto the N atom of NO occurring on the doublet surfaces, state-averaged CASSCF(11,11) calculations for the two lower-lying electronic states, 1²A'' and 2²A'' (or 1²A' and 2²A'), were first used to obtain the optimized geometries at each fixed C–N bond distance under the constraint of a C_s symmetry, followed directly by single-point calculations using the CASPT2 method for the two distinct electronic states 1²A'' and 2²A'' (or 1²A' and 2²A'), in order to refine the potential energy curves. Finally, the PESs for the reaction considered were constructed using the G2M//B3LYP/6-311+G(3df) and CASPT2/cc-pVTZ//CASSCF/cc-pVDZ relative energies. The B3LYP, MP2, and CCSD(T) calculations were performed using the Gaussian 03 package,²⁰ the CASSCF geometries and vibrational frequencies were computed using the DALTON program,²¹ and the MOLPRO 2002 package²² was used for the scanning CASSCF and CASPT2 calculations. All energies, optimized geometries, zero-point vibrational energies, and rotational constants of all species considered in this article are provided in the Supporting Information

II.2. RRKM/Master Equation Calculations. The G2M//B3LYP/6-311+G(3df) and CASPT2//CASSCF relative energies and the B3LYP/6-311+G(3df) and CASSCF(11,11)/cc-pVDZ harmonic vibrational frequencies obtained above were then used for kinetic analyses. According to the statistical RRKM theory of unimolecular reaction rates,^{23–27} the microcanonical rate constant, $k(E)$, can be expressed as

$$k(E) = \frac{\alpha}{h} \frac{G^\ddagger(E - E^\ddagger)}{\rho(E)}$$

where α is the reaction pathway degeneracy, h is Planck's constant, $G^\ddagger(E - E^\ddagger)$ is the sum of vibrational states of the transition structure counted for energies from 0 to $E - E^\ddagger$, and $\rho(E)$ is the density of vibrational states for a reactant molecule with internal energy E . $G^\ddagger(E - E^\ddagger)$ and $\rho(E)$ were counted with a grain size of 1 cm⁻¹ using the Beyer–Swinehart–Stein–Rabinovith algorithm.²⁸

The product distribution for the CF₂(a³B₁) + NO reaction was obtained by solving the energy-grained master equation under various conditions [$P(\text{He}) = 1\text{--}20$ Torr or 1 atm, $T = 298\text{--}600$ K], including those of the experimental studies.⁸ The Lennard-Jones collision parameters for the bath gas He are $\sigma(\text{He}) = 2.55$ Å and $\epsilon/k_B(\text{He}) = 10$ K.²⁹ Because no collision parameters of [CF₂NO] are available in the literature, the values $\sigma(\text{CF}_2\text{NO}) = 4.4$ Å and $\epsilon/k_B(\text{CF}_2\text{NO}) = 166$ K were estimated based on those of CF₄.²⁹ Troe's biexponential model³⁰ was used for the energy-transfer process, in which an average energy transferred per collision, $\langle \Delta E \rangle_{\text{all}}$, of -130 cm⁻¹ was adopted.²⁹ The probability density function of the energy distribution of formation of the initial adduct was derived by temporarily considering thermodynamic equilibrium between the initial reactants, CF₂(³B₁) + NO, and the nascent adduct, **Iso3a**, CF₂NO. Even at a pressure of 1 atm, the collisional stabilization rates of the chemically activated intermediates involved, with nascent internal energies from ~ 20 to over 70 kcal/mol, are at most $\sim 3 \times 10^8$ s⁻¹, i.e., many orders of magnitude below the computed $(1\text{--}10) \times 10^{12}$ s⁻¹ microcanonical rates of their

dominant unimolecular dissociation reactions (see the next section). In addition, gas temperatures in low-pressure fluorocarbon plasmas are generally low (400–600 K), such that an approximation of collision-free conditions and low reactant energies (as in molecular beam experiments) is valid in this case. Therefore, the product distributions for the title reaction were studied under collision-free conditions as well. In addition to various product branching ratios, thermal rate coefficients can be extracted from a solution of the master equation. The application of master equation methods to problems in gas-phase chemical kinetics, such as combustion, atmospheric chemistry, and chemical vapor deposition, has been discussed in detail in two recent excellent reviews by Miller, Klippenstein, and co-workers.³¹

In the energy-grained master equation for this application, the maximum energy considered was 70000 cm⁻¹ above that of the lowest conformer (e.g., c-F₂CNO), and a very small energy band size of 10 cm⁻¹ was chosen to ensure that the density of states did not change within the band. A stochastic simulation was used to solve the master equation following Gillespie's exact stochastic algorithm.³² To obtain product distributions with high precision, a large number of stochastic trials was chosen, $\sim 10^7$. Choice of a good uniformly distributed random-number generator (RNG) is also very important in stochastic simulations. In this application, various RNGs with a very long period were chosen, including MRG32k3a recommended by L'Ecuyer,³³ RANLUX with a luxury level of 4 by James and Luscher,³⁴ and MT19937 by Matsumoto et al.³⁵ The results obtained were in excellent agreement with each other. A detailed explanation on the stochastic solution of the master equation was given previously,³⁶ and our implementation was described in a recent work.³⁷ It is worth noting here that another ESM implementation is also available in the literature, the MultiWell program suite developed by Barker.³⁸ In addition to the ESM approach, solution of master equation can be gained using deterministic techniques. Some software packages available employing these techniques are ChemRate,³⁹ Unimol,⁴⁰ and VariFlex.⁴¹

III. Results and Discussion

Coupling between the triplet excited CF₂ and the doublet NO can generate chemically activated adducts that have total spin states⁴² of 1/2 or 3/2. As such, the CF₂(a³B₁) + NO reaction could, in principle, proceed on both quartet and doublet electronic state PESs.

III.1. Quartet PES. The quartet electronic PES for the CF₂(a³B₁) + NO reaction was constructed and is schematically presented in Figure 1. In the first reaction step, addition of CF₂(a³B₁) to the N end of NO faces an energy barrier of 1.3 kcal mol⁻¹ to form F₂CNO(⁴A''), **Iso1**, via **TS1**. **TS1** does not exist at the B3LYP level, but was located at the MP2/6-311+G(d) level. To check the existence of **TS1** at a higher level of theory, we carried out IRC calculations using the MP2 method and then computed single-point electronic energies at the CCSD(T)/6-311G(d) level. The results plotted in Figure 2 verify that **TS1** really exists. The F₂CNO, **Iso1**, then decomposes via **TS3** with a barrier height of 36.5 kcal mol⁻¹, leading to O(³P) + F₂CN. **TS3** lies 5.1 kcal mol⁻¹ above **TS1** and is geometrically tighter. As a result, redissociation of **Iso1** back to the initial reactants is expected to be favored over its decomposition to O(³P) + F₂CN. To evaluate the ratio of the fractions of the products CF₂(a³B₁) + NO and O(X³P) + F₂CN as a function of temperature, we solved the master equation (at $P = 20$ Torr). The results presented in Figure 3 show that, even at 1000 K, the yield of

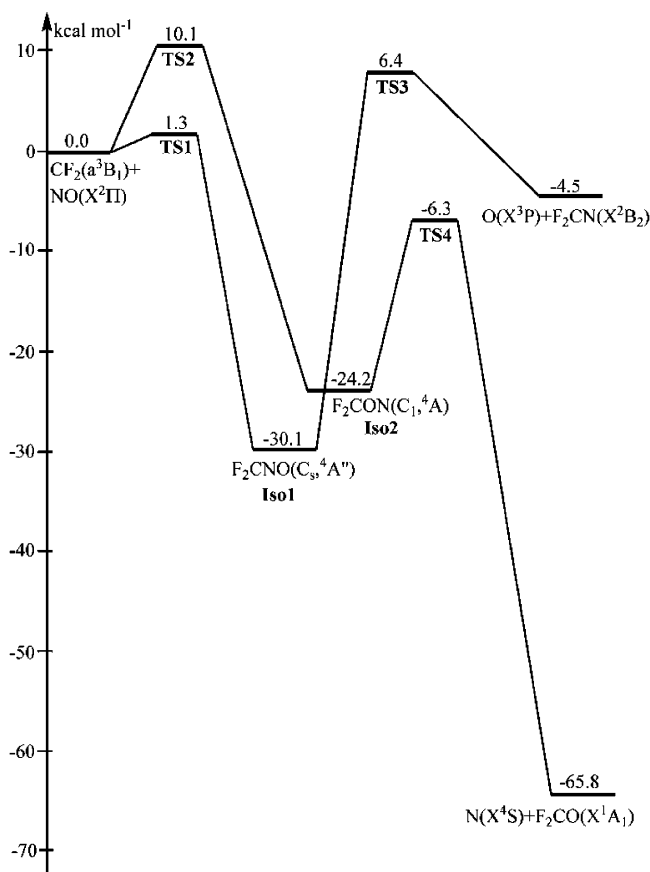


Figure 1. Quartet electronic state PES of the CF₂(a³B₁) + NO(X²Π) reaction constructed using the G2M relative energies.

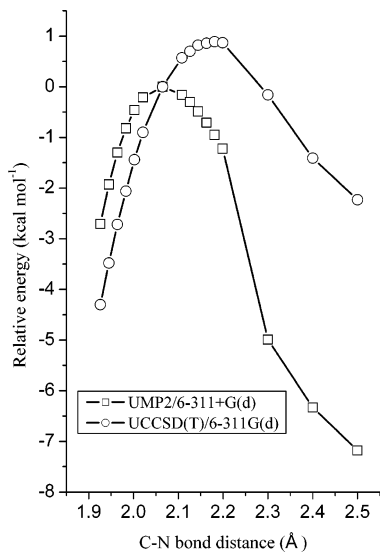


Figure 2. Minimum-energy pathway computed at the MP2/6-311+G(d) and CCSD(T)/6-311G(d) levels of theory for the channel CF₂(a³B₁) + NO(X²Π) → F₂CNO(⁴A'').

redissociation back to the reactants [CF₂(a³B₁) + NO] is still about 200 times larger than the yield of decomposition to O(³P) + F₂CN. As a result, the latter reaction channel is apparently not important under relevant reaction conditions.

The CF₂(a³B₁) carbene can attack the O end of NO via TS2, leading to F₂CON(⁴A), Iso2. This step must overcome a barrier of 10.1 kcal mol⁻¹. Iso2 then decomposes rapidly to yield the most exothermic products, N(⁴S) + F₂CO, via the lower-lying TS4 with a barrier height of 17.9 kcal mol⁻¹. However, TS2 lies 8.8 kcal mol⁻¹ above TS1 and is also geometrically tighter.

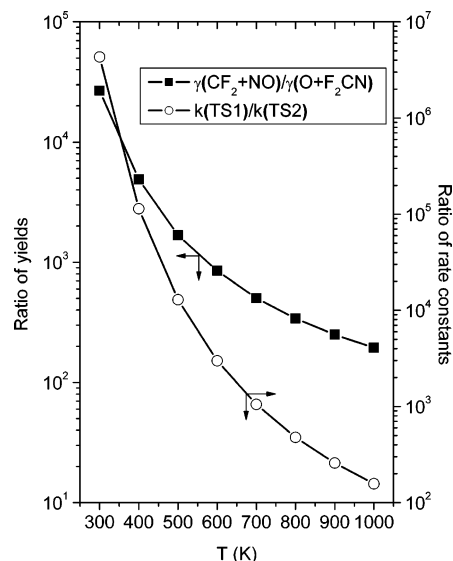


Figure 3. CF₂(a³B₁) + NO(X²Π) reaction on the quartet electronic state PES: (○) rate constant ratio for the CF₂(a³B₁) + NO entrance channels versus temperature, (■) yield ratio of the (re-)decomposition channels of F₂CNO(⁴A'') versus temperature.

Kinetic calculations using TST theory^{23–27} show that (see Figure 3), at 1000 K, the rate of the entrance reaction channel via TS2 is about 160 times lower than that via TS1. As a consequence, the former path cannot efficiently compete with the latter at relevant temperatures.

In summary, although the CF₂(a³B₁) + NO reaction can occur on the quartet PES, the initial addition step needs to overcome a non-negligible energy barrier, and furthermore, the subsequent decomposition of F₂CNO(⁴A''), Iso1, to the final products O(³P) + F₂CN is energetically much less favorable than its redissociation back into the reactants. As a result, the reaction proceeding on the quartet surface is not expected to contribute significantly to the overall rate. Therefore, N(⁴S) + F₂CO are unlikely to be formed even though they are, thermodynamically, the most favorable products.

III.2. Doublet PES. The combination of triplet excited CF₂ with NO, under imposed C_s minimum symmetry, occurs on two higher-lying excited doublet electronic PESs (2²A'' and 2²A'), whereas the reaction of singlet ground-state CF₂ with NO takes place on two low-lying doublet electronic states (1²A'' and 1²A'). First, to estimate the energies of these ground and excited states as a function of the distance r(C–N), scanning calculations using multireference methods such as CASPT2 and CASSCF are necessary, even though the accuracy of these levels is limited because one has to resort to state-averaged wavefunctions. Second, the complexity of the system of energy surfaces forced us to impose the C_s point group as minimum symmetry, so as to limit the number of states for a given wavefunction symmetry; if the C₁ point group were allowed, one would be faced with four different electronic states, but it proved rather difficult to construct the higher-lying states without symmetry. The higher states could, in principle, be calculated as the higher roots of the CASSCF wavefunctions, but the identity of the states considered could not be determined appropriately, and this unavoidably results in even larger errors on the energies. The IRCMax(CASPT2/CASSCF) calculations presented in Figure 4 show that the interaction of triplet CF₂(a³B₁) with NO gives rise to an attractive 2²A'' F₂CNO surface and a repulsive 2²A' surface. That this reaction can occur on an attractive surface (2²A'') is fully consistent with the high rate coefficient and the negative temperature dependence observed by us.⁸ The com-

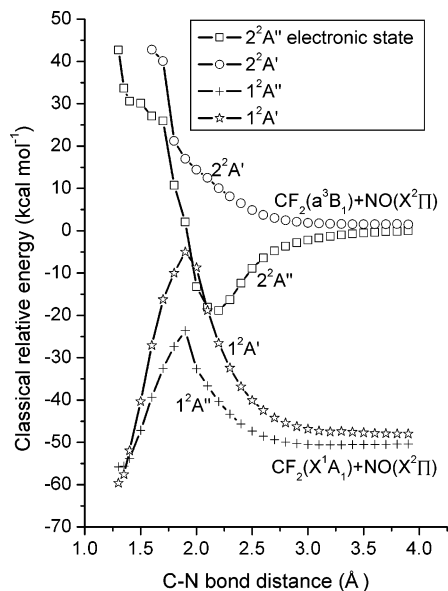
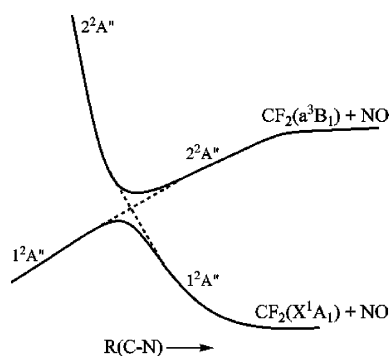


Figure 4. IRCMax[CASPT2/CASSCF/6-311G(d)] calculations for the entrance channels of the CF₂(a³B₁) + NO(X²Π) reaction on the 2²A'' and 2²A' (B-O) surfaces and for those of the CF₂(X¹A₁) + NO(X²Π) reaction on the 1²A'' and 1²A' (B-O) surfaces.

SCHEME 1



bination of singlet ground-state CF₂ with NO, on the other hand, can proceed only on the (low-lying) repulsive surfaces 1²A'' and 1²A'.

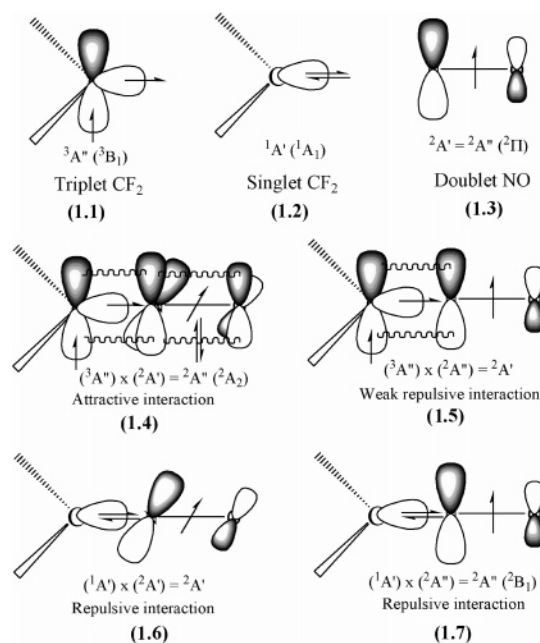
The CASPT2/CASSCF(11,11) results displayed in Figure 4 can be interpreted as follows:

(i) The upper and lower 2²A'' surfaces under C_s symmetry result, in fact, from an avoided crossing imposed by the Born–Oppenheimer (B–O) approximation, as illustrated by Scheme 1. The B–O-allowed intersecting curves (dashed lines) schematically represent the 2A₂-state bonding interaction of triplet CF₂ with NO and the repulsive 2B₁-state antibonding interaction, both under the higher C_{2v} symmetry.

(ii) In the reaction of CF₂(X¹A₁) with NO under C_s symmetry (CNO plane), there are no bonding interactions between the σ lone pair of CF₂(X¹A₁) and the half-occupied π valence orbital of NO (see Chart 1, parts 1.6 and 1.7). Instead, there is a repulsive interaction between the σ lone pairs of CF₂(X¹A₁) and NO, which leads to the purely repulsive 1²A'' and 1²A' surfaces.

(iii) Interaction of CF₂(a³B₁) with NO can occur on both the 2²A'' and 2²A' electronic surfaces (where the prefixes 1 and 2 refer to the successive electronic states, of the given symmetry, in the B–O frame). In the 2²A'' state, there is a bonding interaction of the unpaired pπ orbital of CF₂ with the filled π orbital of NO resulting in three π electrons delocalized over three atoms (see Chart 1, part 1.4). As a result, the 2²A'' surface is attractive. In the 2²A' state, there is a (weaker) π-bonding

CHART 1



overlap of the half-occupied (p)π orbitals of CF₂(a³B₁) and NO, which is overridden by the stronger repulsion between the half-occupied σ orbital of CF₂(a³B₁) and the in-plane σ lone pair of N (see Chart 1, part 1.5). Hence, the 2²A' surface is moderately repulsive.

Therefore, as shown in Figure 4, the reaction of CF₂(a³B₁) with NO first takes place on the 2²A'' attractive surface, leading to the excited doublet adduct F₂C–NO, which has an internal energy of ~19 kcal mol⁻¹ at the CASPT2/6-311G(d) level. The equilibrium C–N bond distance in this adduct is about ~2.1 Å. Around the equilibrium position of this adduct (i.e., in the harmonic-oscillator region), there is an extensive overlap of the 2²A'' and 1²A' B–O surfaces, the potential energy of the 2²A'' state being nearly equal to that of 1²A'. At the high kinetic energies of the nuclei involved here—the potential energy of the overlap region lying some 15 kcal mol⁻¹ below the reactant level—this should result in a high probability of a Landau–Zener transition from the 2²A'' surface to the 1²A' surface. To estimate this transition probability, we computed the energy gap 2a between these two states at the C–N bond distance of 2.1 Å for the CASSCF-optimized geometry of the 2²A'' state, obtaining 2.5 kcal mol⁻¹ at the CASPT2 level. The Landau–Zener transition probability P is given by the expression⁴³

$$P = \exp\left(-\frac{2\pi a^2}{\Delta F \hbar u}\right)$$

where a is one-half of the energy gap, a = 1.25 kcal mol⁻¹; u is the relative velocity of the nuclei at the point of “intersection”, u ≈ 3 × 10⁵ cm s⁻¹; and ΔF is the difference in the potential energy gradients of the two intersecting surfaces, estimated at ΔF ≈ 150 kcal mol⁻¹ Å⁻¹. We thus find P = exp(-0.14) = 0.87; i.e., transition occurs at almost each C–N vibration.

The vibrating doublet F₂C–NO adduct, once on the 1²A' electronic surface after transition from the 2²A'' surface, will either elongate and thus spontaneously decompose into CF₂(X¹A₁) + NO products in the direct “chemical quenching” mechanism described above or contract and then relax to the doublet F₂CNO(X²A') ground state, i.e., the F₂CNO(1²A') structure for r(C–N) ≈ 1.3 Å in Figure 4, denoted as Iso3a in Figure 5. However, the latter C–N contraction step faces a

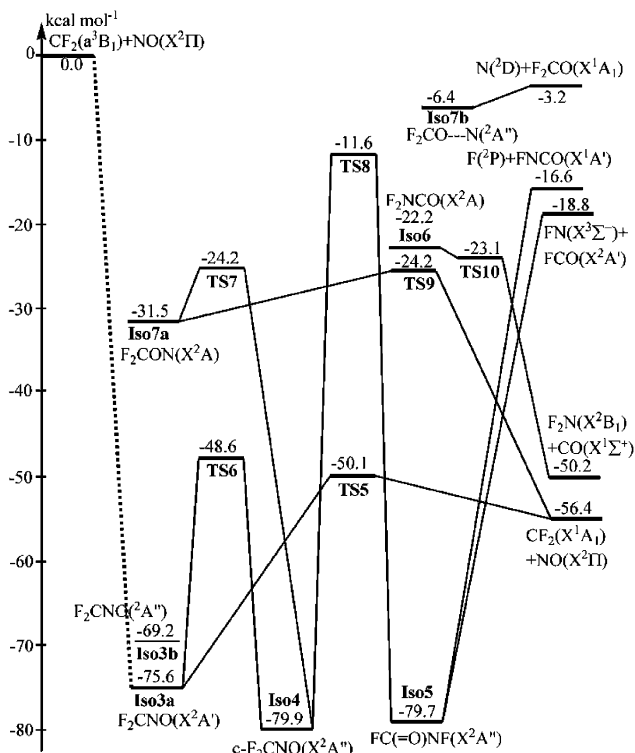


Figure 5. Lowest-lying doublet electronic state PES of the CF₂(a³B₁) + NO(X²Π) reaction constructed using the G2M and CASPT2 relative energies. The dotted line indicates that the CF₂(a³B₁) + NO → F₂CNO(X²A') entrance channel proceeds indirectly via the doublet excited adduct F₂CNO(2²A'') (see text).

potential energy maximum that lies about 10 kcal/mol above the crossing region (see Figure 4) and therefore appears less favorable than the former. Another pathway for the initial F₂CNO adduct that could lead indirectly to **Iso3a**, F₂CNO(X²A'), might involve the B–O-allowed “conical” intersection of the two 2²A'' surfaces along their higher-symmetry C_{2v} cross section, schematized by the dashed curves in Scheme 1, which represent the attractive C_{2v} 2²A₂ and repulsive C_{2v} 2²B₁ states (see also Chart 1). The F₂CNO(1²A'') structure that would result (denoted **Iso3b** in Figure 5) could then rapidly relax to the F₂CNO(X²A') ground state by internal conversion. However, our IRCMax[CASPT2/CASSCF/6-311G(d)] results (see Figure 4) show clearly that the lowest-energy state of the initial, attractive F₂C–NO adduct is the lower-symmetry C_s 2²A'' state rather than the higher-symmetry C_{2v} 2²A₂ state, such that the 2²A'' minimum, in fact, lies lower in energy than the C_{2v} 2²A₂ and C_{2v} 2²B₁ intersection, implying that the upper cone of Scheme 1 is strongly distorted, with two deep sags, to the left and right of the C_{2v} section. As a result, the preferred minimum-energy pathways of the initial adduct should not follow the C_{2v} 2²A₂ curve and therefore also miss the conical intersection with the repulsive C_{2v} 2²B₁ curve.

It should be stressed that, in the foregoing discussion, a symmetry of at least C_s was imposed in the vicinity of the crossing points, because the energies for the minima (along the C–N reaction coordinate) of the C₁ energy surfaces could not be evaluated. Although it is not possible to estimate the precise consequences of relaxing this constraint, it should be noted that all doublet C₁ states are of the same species and therefore should avoid mutual crossings under the B–O approximation.

Let us now consider the lowest-lying doublet electronic PES for this reaction, which is schematically illustrated in Figure 5. The F₂CNO(C_s, X²A'), **Iso3a**, formed indirectly from the combination of CF₂(a³B₁) with NO belongs to the C_s point group

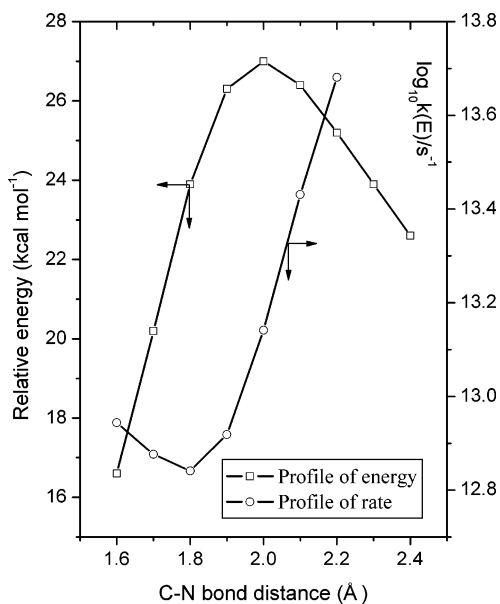


Figure 6. Energy profile for the channel F₂CNO(X²A') → CF₂(X¹A₁) + NO(X²Π) computed at the G2M level and profile of the variational microcanonical rate constant at a total energy corresponding to the CF₂(a³B₁) + NO reactant limit. Note that only the minimum rate constant, at the reaction bottleneck, of ~7 × 10¹² s⁻¹, has physical meaning.

and lies 75.6 kcal mol⁻¹ lower in energy than the reactants. The 2²A'' excited electronic state of F₂CNO, denoted as **Iso3b**, lies only 6.4 kcal mol⁻¹ higher than the ground electronic state **Iso3a**. **Iso3b**, if produced from the initial reactants, is expected to immediately undergo an internal conversion into **Iso3a**. The dominant fate of **Iso3a** is a facile C–N bond dissociation via the loose, product-like TS5(2²A'), which lies only 25.5 kcal mol⁻¹ above **Iso3a**, to yield the low-energy products CF₂(X¹A₁) + NO. Thus, overall, this path results in chemical quenching of CF₂(a³B₁) by NO. IRC calculations along the C–N reaction coordinate were subsequently performed to determine the variational microcanonical RRKM rate constant for a total energy corresponding to the reactant limit (i.e., collision-free conditions at 0 K). The results are plotted in Figure 6. The C–N bond distance in TS5 is 2.2 Å at the B3LYP/6-311+G(3df) level but 2.0 Å at the G2M level. RRKM calculations generate a variational TS with a C–N distance of 1.8 Å. Concomitantly, the “true” variational rate constant, of ~7 × 10¹² s⁻¹, is about 5 times less than that computed for the conventional maximum-energy transition structure. Note that this variational *k*(*E*) value surpasses the rate of intramolecular vibrational relaxation (~10¹² s⁻¹), such that the statistical RRKM theory should break down. However, the F₂C–NO dissociation process at issue does not require any vibrational-energy redistribution, because the hot **Iso3a** arises here by CF₂(a³B₁) + NO combination that should activate precisely the C–N vibration mode of interest. As a result, the statistical, variational *k*(*E*) value of ~7 × 10¹² s⁻¹ should rather be a lower limit, with the C–N vibration frequency of ~3 × 10¹³ s⁻¹ as upper limit.

A second possible pathway from **Iso3a** forms cyclic c-F₂CNO (**Iso4**) via TS6 (27 kcal mol⁻¹ above **Iso3a**). TS6 has no symmetry and is rather tight. At first sight, it is somewhat surprising that TS6 connects **Iso3a**(X²A') to **Iso4**(X²A''). However, IRC calculations at the B3LYP/6-311+G(3df) level confirmed this connection (cf. Figure 7). A similar conclusion was obtained earlier for the CH₂(X³B₁) + NO reaction.¹¹ This is merely due to a change in the molecular plane.

Iso4 can rearrange back to **Iso3a** via TS6 with a barrier height of 31.3 kcal mol⁻¹ or undergo a further ring-opening to form

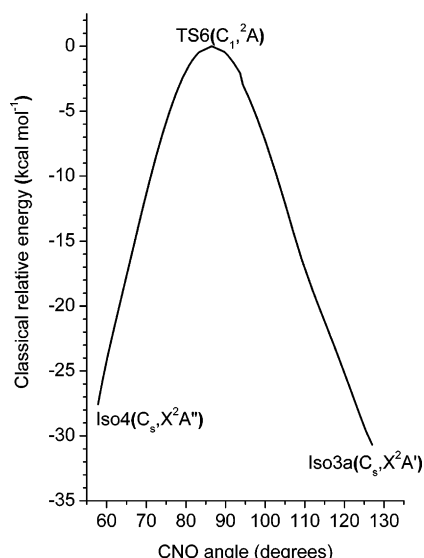


Figure 7. Minimum-energy pathway for the $F_2CNO(X^2A') \rightarrow c-F_2CNO(X^2A'')$ step computed at the B3LYP/6-311+G(3df) level of theory.

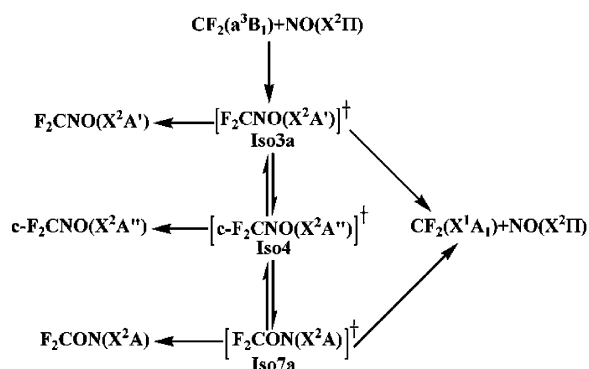


Figure 8. Kinetic scheme used for RRKM/ME calculations for the $CF_2(a^3B_1) + NO$ reaction occurring on the lowest-lying doublet electronic state PES.

Iso7a via **TS7**, which lies 55.7 and 7.3 kcal mol⁻¹ above **Iso4** and **Iso7a**, respectively, as calculated at the CASPT2 level of theory. CASSCF calculations for **TS7** resulted in three significant configurations with different coefficients of -0.7, 0.5, and 0.4, indicating a multireference character. Isomerization of **Iso4** to $FC(=O)NF$, **Iso5**, by concerted breaking of the N–O bond and 1,2-F shift from C to N must proceed through the very tight and high-energy **TS8** (barrier of 68.3 kcal mol⁻¹) and is therefore unlikely to be of any importance. If formed at all, **Iso5** can dissociate by breaking the C–N or C–F bond, leading to $FN(^3\Sigma_g^-) + FCO$ or $F(^2P) + FNCO$, respectively. We were not successful in locating a transition structure for the alternative

rearrangement of **Iso5** to F_2NCO **Iso6** by a 1,2-F shift from the N atom to the C atom, which should be followed by spontaneous fragmentation into $F_2N + CO$.

$F_2CON(C_1)$, **Iso7a**, lies 31.5 kcal mol⁻¹ below the reactants (CASPT2). It has a two-configuration wavefunction (coefficients of -0.79 and 0.45) and could either go back to **Iso4** via **TS7** or break the C–O bond to yield the products $CF_2(X^1A_1) + NO$ via **TS9**, which lies 7.3 kcal mol⁻¹ above **Iso7a**. With a C–O bond only 0.29 Å longer than that in **Iso7a**, **TS9** is an early and reactant-like transition structure. Another conformer is **Iso7b**(^{2A''}), with a long O–N distance of 1.6 Å, lying 3.2 kcal mol⁻¹ below $N(^2D) + F_2CO$, suggesting a weak complex by loose combination of $N(^2D)$ and F_2CO .

In summary, the $CF_2(a^3B_1) + NO$ reaction, proceeding indirectly through the vibrationally excited intermediate $F_2CNO(X^2A')$, yields only $CF_2(X^1A_1) + NO$ as major products. However, the decomposition of $F_2CNO(X^2A')$ to $CF_2(X^1A_1) + NO$ can proceed either via simple C–N homolysis or via the *c*- F_2CNO and F_2CON isomers in a more involved route. It is interesting to quantitatively evaluate the competition between these two channels. The reaction scheme for the kinetic analysis is presented in Figure 8. The G2M and CASPT2/CASSCF(11,-11) energies and CASSCF vibrational frequencies were used to compute the microcanonical rate constants. The master equation under various reaction conditions was solved using the exact stochastic simulation method. The product distributions were found to be pressure-independent (<100 atm), but exhibited very slight changes as a function of temperature (cf. Table 2). Therefore, the product distribution computed under collision-free conditions at $T = 0$ K appears to be valid in the pressure and temperature ranges of interest. At $P = 1$ atm and room temperature, the obtained product distribution shows that dissociation of F_2CNO by C–N homolysis via **TS5** contributes 99.7% (as a lower limit; see above), whereas the remaining 0.3% arises from decomposition involving intermediates.

It can thus be concluded that the $CF_2(a^3B_1) + NO$ reaction almost exclusively yields $CF_2(X^1A_1) + NO$ as products via chemical quenching paths.

IV. Conclusions

The fast $CF_2(a^3B_1) + NO$ reaction was theoretically studied to elucidate the reaction mechanisms involved and to evaluate the product distributions. Various quantum chemical methods in conjunction with different basis sets were used to construct PESs. On the basis of G2M and CASPT2 relative energies, approximate Landau–Zener transition probabilities between crucial “avoided-crossing” PESs were evaluated. Also, RRKM microcanonical rate constants of relevant unimolecular reaction steps were computed, and product distributions were estimated by master equation analysis using the exact stochastic simulation

TABLE 2: RRKM/ME-Computed Product Distribution (%) for the $CF_2(a^3B_1) + NO(X^2II)$ Reaction Proceeding through the Ground-State Doublet Equilibrium Structure $F_2CNO(X^2A')$, **Iso3a, under Various Reaction Conditions**

reaction conditions	collisionally stabilized F_2CNO	$CF_2(X^1A_1) + NO(X^2II)$ from direct F_2CNO^* dissociation ^a	$CF_2(X^1A_1) + NO(X^2II)$ from F_2CNO^* through the F_2CON^* isomer
T = 0 K, P = 0 Torr	0	99.76	0.24
T = 298 K, P = 0 Torr	0	99.71	0.29
T = 298 K, P = 1 Torr	0	99.71	0.29
T = 298 K, P = 20 Torr	0	99.71	0.29
T = 298 K, P = 760 Torr	0	99.71	0.29
T = 600 K, P = 0 Torr	0	99.59	0.41
T = 600 K, P = 1 Torr	0	99.59	0.41
T = 600 K, P = 20 Torr	0	99.59	0.41
T = 600 K, P = 760 Torr	0	99.59	0.41

^a As lower limits; see text.

method. The main results emerging from this study can be summarized as follows:

(1) The CF₂(a³B₁) + NO reaction on the two quartet energy surfaces, ⁴A and ⁴A'', is negligibly slow at moderate temperatures because either the initial addition step (⁴A surface) or the subsequent decomposition step (⁴A'' surface) faces substantial effective energy barriers, of ~10 and ~6 kcal mol⁻¹, respectively.

(2) On the other hand, CF₂(a³B₁) and NO rapidly combine on the barrier-free, attractive ²A'' doublet energy surface to form the electronically excited adduct F₂CNO(²A''). The resulting high relative F₂C–NO velocity at the ²A'' energy minimum together with the close proximity (~2.5 kcal mol⁻¹) there of the lower-lying repulsive ¹A' surface, give rise to a high Landau–Zener ²A'' → ¹A' transition probability of about 90% at each avoided-crossing C–N vibration. Given that the repulsive F₂CNO(¹A') state connects to the ground-state products CF₂(X¹A₁) + NO(²Π), a major, if not dominant, CF₂(a³B₁) + NO reaction channel is therefore expected to be fast direct chemical quenching CF₂(a³B₁) → X¹A₁ by NO.

(3) In an alternative route, the F₂CNO(¹A') adduct can relax to its ground-state equilibrium structure, F₂CNO(X²A'). The latter also rapidly produces CF₂(X¹A₁) + NO, with a yield close to unity, which amounts to indirect chemical quenching.

(4) Simultaneous physical quenching of electronically excited CF₂(a³B₁) by collision with NO, directly leading to CF₂(X¹A₁) + NO, might also occur. Yet, available experimental data^{5,6,8} clearly indicate that rates of physical quenching cannot match the high reaction rate observed and theoretically rationalized as fast chemical quenching.

(5) The most remarkable result obtained in this work is perhaps a crossing probability of about 90% per vibration between two avoided potential energy surfaces. This suggests that, in the real world of chemically activated reactions, with extremely fast-moving nuclei, the separation of energy surfaces and the avoided crossing between them as a consequence of the Born–Oppenheimer approximation lose their meaning for specific cases.

Acknowledgment. The authors thank the FWO-Vlaanderen and the KULeuven Research Council (GOA program and BOF fund) for continuing financial support. T.L.N. thanks the KULeuven Research Council for a postdoctoral mandate.

Supporting Information Available: Complete listing of the quantum chemical results, containing product distributions, IRC calculations, the most important coefficients in the wavefunctions, geometries, rotational constants, vibrational wave numbers, and energy parameters, for all structures discussed in the text, as well as minimum structures, transition structures, and stationary-point structures. This material is available free of charge via the Internet at <http://pubs.acs.org>.

References and Notes

- (1) (a) Leopold, D. G.; Murray, D. D.; Miller, A. E. S.; Lineberger, W. C. *J. Chem. Phys.* **1985**, *83*, 4849. (b) Matus, M. H.; Nguyen, M. T.; Dixon, D. A. *J. Phys. Chem. A* **2006**, *110*, 8864 and references therein.
- (2) Koda, S. *Chem. Phys. Lett.* **1978**, *55*, 353.
- (3) Mckellar, A. R.; P. R. Bunker, P. R.; Sears, P. R.; Evenson, K. M.; Saykally, R. M.; Langhoff, S. R. *J. Chem. Phys.* **1983**, *79*, 5251.
- (4) (a) Hack, W.; Wagner, M.; Hoyermann, K. *J. Phys. Chem.* **1995**, *99*, 10847; Yamasaki, K.; Tanaka, A.; Watanabe, A.; Yokoyama, K.; Tokue, I. *J. Phys. Chem.* **1995**, *99*, 15086. (b) Modica, A. P. *J. Chem. Phys.* **1967**, *46*, 3663. (c) Edelbuttel-Einhaus, J.; Hoyermann, K.; Rohde, G.; Wagner, H. G. *Ber. Bunsen-Ges. Phys. Chem.* **1989**, *93*, 1413. (d) Dalby, F. W. J. *Chem. Phys.* **1964**, *41*, 2065.
- (5) Koda, S. *J. Phys. Chem.* **1979**, *83*, 2065.
- (6) Young, R. A.; Blauer, J.; Bower, R.; Lin, C. L. *J. Chem. Phys.* **1988**, *88*, 4834.
- (7) Rozum, I.; Mason, N. T.; Tennyson, J. *J. Phys. B: At. Mol. Opt. Phys.* **2002**, *35*, 1583.
- (8) (a) Dils, B.; Elsamra, R. M. I.; Peeters, J.; Carl, S. A. *Phys. Chem. Chem. Phys.* **2003**, *5*, 5405. (b) Hou, X. J.; Nguyen, T. L.; Carl, S. A.; Peeters, J.; Nguyen, M. T. *Chem. Phys. Lett.* **2005**, *402*, 460.
- (9) Fikri, M.; Meyer, S.; Roggenbuck, J.; Temps, F. *Faraday Discuss.* **2001**, *119*, 223.
- (10) (a) Shapley, W. A.; Bacskay, G. B. *Theor. Chem. Acc.* **1998**, *100*, 212. (b) Shapley, W. A.; Bacskay, G. B. *J. Phys. Chem. A* **1999**, *103*, 4505. (c) Shapley, W. A.; Bacskay, G. B. *J. Phys. Chem. A* **1999**, *103*, 4514.
- (11) Su, H.; Kong, F. *J. Chem. Phys.* **2000**, *113*, 1885.
- (12) Becke, A. D. *J. Chem. Phys.* **1993**, *98*, 5648.
- (13) Scott, A. P.; Radom, L. *J. Phys. Chem.* **1996**, *100*, 16502.
- (14) Pople, J. A.; Head-Gordon, M.; Raghavachari, K. *J. Chem. Phys.* **1987**, *87*, 5968.
- (15) Head-Gordon, M.; Pople, J. A.; Frisch, M. J. *Chem. Phys. Lett.* **1988**, *153*, 503.
- (16) Mebel, A. M.; Morokuma, K.; Lin, M. C. *J. Chem. Phys.* **1995**, *103*, 7414.
- (17) (a) Pople, J. A.; Head-Gordon, M.; Fox, D. J.; Raghavachari, K.; Curtiss, L. A. *J. Chem. Phys.* **1989**, *90*, 5622. (b) Curtiss, L. A.; Raghavachari, K.; Trucks, G. W.; Pople, J. A. *J. Chem. Phys.* **1991**, *94*, 7221.
- (18) Lee, T. J.; Taylor, P. R. *Int. J. Quantum Chem. Symp.* **1989**, *23*, 199.
- (19) (a) Werner, H. P. *Mol. Phys.* **1996**, *89*, 645. (b) Celani, P.; Werner, H. P. *J. Chem. Phys.* **2000**, *112*, 5546.
- (20) (a) Frisch, M. J.; Trucks, G. W.; Schlegel, H. B.; Scuseria, G. E.; Robb, M. A.; Cheeseman, J. R.; Zakrzewski, V. G.; Montgomery, J. A., Jr.; Stratmann, R. E.; Burant, J. C.; Dapprich, S.; Millam, J. M.; Daniels, A. D.; Kudin, K. N.; Strain, M. C.; Farkas, O.; Tomasi, J.; Barone, V.; Cossi, M.; Cammi, R.; Mennucci, B.; Pomelli, C.; Adamo, C.; Clifford, S.; Ochterski, J.; Petersson, G. A.; Ayala, P. Y.; Cui, Q.; Morokuma, K.; Malick, D. K.; Rabuck, A. D.; Raghavachari, K.; Foresman, J. B.; Cioslowski, J.; Ortiz, J. V.; Stefanov, B. B.; Liu, G.; Liashenko, A.; Piskorz, P.; Komaromi, I.; Gomperts, R.; Martin, R. L.; Keith, T.; Al-Laham, M. A.; Peng, C. Y.; Nanayakkara, A.; Gonzalez, C.; Challacombe, M.; Gill, P. M. W.; Johnson, B. G.; Chen, W.; Wong, M. W.; Andres, J. L.; Head-Gordon, M.; Replogle, E. S.; Pople, J. A. *Gaussian 98*; Gaussian, Inc.: Pittsburgh, PA, 1998. (b) Frisch, M. J.; Trucks, G. W.; Schlegel, H. B.; Scuseria, G. E.; Robb, M. A.; Cheeseman, J. R.; Montgomery, J. A., Jr.; Vreven, T.; Kudin, K. N.; Burant, J. C.; Millam, J. M.; Iyengar, S. S.; Tomasi, J.; Barone, V.; Mennucci, B.; Cossi, M.; Scalmani, G.; Rega, N.; Petersson, G. A.; Nakatsuji, H.; Hada, M.; Ehara, M.; Toyota, K.; Fukuda, R.; Hasegawa, J.; Ishida, M.; Nakajima, T.; Honda, Y.; Kitao, O.; Nakai, H.; Klene, M.; Li, X.; Knox, J. E.; Hratchian, H. P.; Cross, J. B.; Bakken, V.; Adamo, C.; Jaramillo, J.; Gomperts, R.; Stratmann, R. E.; Yazyev, O.; Austin, A. J.; Cammi, R.; Pomelli, C.; Ochterski, J. W.; Ayala, P. Y.; Morokuma, K.; Voth, G. A.; Salvador, P.; Dannenberg, J. J.; Zakrzewski, V. G.; Dapprich, S.; Daniels, A. D.; Strain, M. C.; Farkas, O.; Malick, D. K.; Rabuck, A. D.; Raghavachari, K.; Foresman, J. B.; Ortiz, J. V.; Cui, Q.; Baboul, A. G.; Clifford, S.; Cioslowski, J.; Stefanov, B. B.; Liu, G.; Liashenko, A.; Piskorz, P.; Komaromi, I.; Martin, R. L.; Fox, D. J.; Keith, T.; Al-Laham, M. A.; Peng, C. Y.; Nanayakkara, A.; Challacombe, M.; Gill, P. M. W.; Johnson, B.; Chen, W.; Wong, M. W.; Gonzalez, C.; Pople, J. A. *Gaussian 03*; Gaussian, Inc.: Pittsburgh, PA, 2003.
- (21) Helgaker, T.; Jensen, H. J. Aa.; Jørgensen, P.; Olsen, J.; Ruud, K.; Ågren, H.; Auer, A. A.; Bak, K. L.; Bakken, V.; Christiansen, O.; Coriani, S.; Dahle, P.; Dalskov, E. K.; Enevoldsen, T.; Fernandez, B.; Hättig, C.; Hald, K.; Halkier, A.; Heiberg, H.; Helttema, H.; Jonsson, D.; Kirpekar, S.; Kobayashi, R.; Koch, H.; Mikkelsen, K. V.; Norman, P.; Packer, M. J.; Pedersen, T. B.; Ruden, T. A.; Sanchez, A.; Saue, T.; Sauer, S. P. A.; Schimmelpfennig, B.; Sylvester-Hvid, K. O.; Taylor, P. R.; Vahtras, O. *DALTON, A Molecular Electronic Structure Program*, release 1.2; National Supercomputer Centre: Linköping, Sweden, 2001.
- (22) *MOLPRO*; Werner, H.-J.; Knowles, P. J.; Lindh, R.; Manby, F. R.; Schütz, M.; Celani, P.; Korona, T.; Rauhut, G.; Amos, R. D.; Bernhardsson, A.; Berning, A.; Cooper, D. L.; Deegan, M. J. O.; Dobbyn, A. J.; Eckert, F.; Hampel, C.; Heter, G.; Lloyd, A. W.; McNicholas, S. J.; Meyer, W.; Mura, M. E.; Nicklass, A.; Palmieri, P.; Pitzer, R.; Schumann, U.; Stoll, H.; Stone, A. J.; Tarroni, R.; Thorsteinsson, T. University College Cardiff Consultants Limited: Cardiff, U.K., 2002.
- (23) (a) Robinson, P.; Holbrook, K. *Unimolecular Reactions*; Wiley-Interscience: London, 1972. (b) Holbrook, K.; Pilling, M.; Robertson, S. *Unimolecular Reactions*, 2nd ed.; Wiley: New York, 1996.
- (24) Forst, W. *Theory of Unimolecular Reactions*; Academic Press: New York, 1973.
- (25) Gilbert, R. G.; Smith, S. C. *Theory of Unimolecular and Recombination Reactions*; Blackwell Scientific: Oxford, U.K., 1990.
- (26) Fernandez-Ramos, A.; Miller, J. A.; Klippenstein, S. J.; Truhlar, D. G. *Chem. Rev.* **2006**, *106*, 4518.

- (27) Steinfeld, J. I.; Francisco, J. S.; Hase, W. L. *Chemical Kinetics and Dynamics*; Prentice Hall: Englewood Cliffs, NJ, 1999.
- (28) (a) Beyer, T.; Swinehart, D. F. *Commun. Assoc. Comput. Mach.* **1973**, *16*, 379. (b) Stein, S. E.; Rabinovitch, B. S. *J. Phys. Chem.* **1973**, *58*, 2438.
- (29) Hippler, H.; Troe, J.; Wendelken, H. J. *J. Chem. Phys.* **1983**, *78*, 6709.
- (30) Troe, J. *J. Chem. Phys.* **1977**, *66*, 4745.
- (31) (a) Miller, J. A.; Klippenstein, S. J. *J. Phys. Chem. A* **2006**, *110*, 10528. (b) Fernandez-Ramos, A.; Miller, J. A.; Klippenstein, S. J.; Truhlar, D. G. *Chem. Rev.* **2006**, *106*, 4518.
- (32) (a) Gillespie, D. T. *J. Comput. Phys.* **1976**, *22*, 403. (b) Gillespie, D. T. *J. Phys. Chem.* **1977**, *81*, 2340. (c) Gillespie, D. T. *J. Comput. Phys.* **1978**, *28*, 395.
- (33) (a) L'Ecuyer, P. *Oper. Res.* **1999**, *47*, 159. (b) L'Ecuyer, P.; Simard, R.; Chen, E. J.; Kelton, W. D. *Oper. Res.* **2002**, *50*, 1073.
- (34) (a) James, F. *Comput. Phys. Commun.* **1994**, *79*, 111. (b) Luscher, M. *Comput. Phys. Commun.* **1994**, *79*, 100.
- (35) Matsumoto, M.; Nishimura, T. *ACM Trans. Model. Comput. Simul.* **1998**, *8*, 3.
- (36) Vereecken, L.; Huyberechts, G.; Peeters, J. *J. Chem. Phys.* **1997**, *106*, 6564.
- (37) Nguyen, T. L. Ph.D. Dissertation, KULeuven, Leuven, Belgium, Dec 2006 (available at <http://hdl.handle.net/1979/433>).
- (38) Barker, J. R. *MultiWell Program Suite*, version 2.06; University of Michigan: Ann Arbor, MI, 2007.
- (39) Morushin, V.; Tsang, W. *ChemRate. A Computational Data Base for Unimolecular Reactions*; National Institute of Standards and Technology: Gaithersburg, MD, 2000.
- (40) Gilbert, R. G.; Jordan, M. J. T.; Smith, S. C. *UNIMOL Program Suite*; University of Sydney: Sydney, Australia, 1990.
- (41) Klippenstein, S. J.; Wagner, A. F.; Robertson, S. H.; Dunbar, R.; Wardlaw, D. M. *VariFlex Software*, version 1.0; Argonne National Laboratory: Argonne, IL, 1999.
- (42) Guillory, W. A. *Introduction to Molecular Structure and Spectroscopy*, Allyn and Bacon: Boston, 1977.
- (43) (a) Landau, L. *Phys. Z.* **1932**, *2*, 46. (b) Zener, C. *Proc. R. Soc. A* **1932**, *137*, 696.
- (44) Pliego, J. R.; De Almeida, W. B.; Celebi, S.; Zhu, Z.; Platz, M. S. *J. Phys. Chem. A* **1999**, *103*, 7481.